Journal of the European Ceramic Society 17 (1997) 3–12

PII: S0955-2219(96)00080-5
0955-2219/97/$17.00

Processing and Properties of AlN Matrix Composite Ceramics Containing Dispersed Hard Materials

Sylvia Burkhardt,[a] Ralf Riedel[a]* & Gerd Müller[b]

[a]Fachgebiet Disperse Feststoffe, Fachbereich Materialwissenschaft, Technische Hochschule Darmstadt, Petersenstraße 23, 64287 Darmstadt, Germany
[b]Fraunhofer Institut für Silicatforschung, Neunerplatz 2, 97082 Würzburg, Germany

(Received 16 January 1996; revised version received 29 March 1996; accepted 2 April 1996)

Abstract

The fabrication of AlN-(Y_2O_3) matrix ceramics reinforced with dispersed TiN or TiB_2 particles is described and the resulting specimens are characterized by their mechanical properties and thermal conductivity.

The microstructures of the TiN-reinforced specimens sintered at 1700°C without isothermal hold show homogeneously distributed TiN particles (≈ 1 μm) in the fine-grained (1–2 μm) AlN matrix. In contrast, the coarse TiB_2 grains (2–3 μm) of the specimens sintered at 1750°C for 60 min are distributed inhomogeneously in the AlN matrix. Furthermore, the surface of the TiB_2 grains reacted to TiN and BN during densification in 0·1 MPa N_2.

The mechanical properties of the AlN-(0·5 wt% Y_2O_3)/5 wt% TiN composites sintered at 1700°C without holding time were determined to be 12·5 GPa, 390 MPa and 3·6 MPa $m^{1/2}$ for the Vickers hardness HV, *the four-point bending strength* σ_B *and the fracture toughness* K_{Ic}, *respectively. The AlN-(4 wt% Y_2O_3)/25 wt% TiN specimen sintered at 1900°C for 60 min gave 10·7 GPa for the Vickers hardness and 270 MPa for the four-point bending strength. The fracture toughness was determined to be 8·3 MPa $m^{1/2}$. In addition, the thermal conductivity of the AlN–TiN composites was of the order of 65 and 105 W m^{-1} K^{-1} for composites sintered at 1700°C without isothermal hold and at 1900°C for 60 min, respectively.*

The AlN-(2 wt% Y_2O_3)/10 wt% TiB_2-containing specimen sintered at 1750°C for 60 min has HV *of 9·5 GPa,* σ_B *of 220 MPa and* K_{Ic} *of 3·7 MPa $m^{1/2}$.*

The influence of fracture mode and intrinsic stresses on the mechanical properties is illustrated and discussed. Finally, the processing of AlN-(4 wt% Y_2O_3) ceramics without reinforcing particles coated with the TiN-particle reinforced AlN is reported. These layered materials exhibit a high thermal conductivity of 150 W m^{-1} K^{-1} inside the body and enhanced hardness, fracture strength and fracture toughness at the surface. © *1996 Elsevier Science Limited.*

1 Introduction

AlN ceramics are attractive materials for application as substrates for electronic devices[1,2] because of their unique combination of intrinsic properties such as high thermal conductivity,[3] high electrical resistivity[4] and a coefficient of thermal expansion similar to that of silicon. In contrast, AlN exhibits low mechanical properties with respect to flexural strength and fracture toughness and has, therefore, not been considered as a candidate material for structural applications. The intention of our work was to develop particle-reinforced AlN-(Y_2O_3) ceramics with improved mechanical properties and high thermal conductivity for use as wear parts, wear-resistant layers and/or cutting tools.

Reinforcement of ceramics in combination with high hardness can be achieved, for example, by dispersing hard materials in the matrix.[5] Therefore, various powder mixtures including Y_2O_3 as sintering aid and up to 35 wt% TiN or TiB_2 addition, combined with two different sintering programmes, were used to obtain composites with both higher flexural strength and hardness (1700°C/0 min) and with higher fracture toughness and thermal conductivity (1900°C/60 min). The upper limit of hard particle addition is given by 35 wt% (~30 vol%) to avoid percolation effects in the electrical conductivity.[6–8]

Additionally, it must be considered that mechanical properties of materials are determined by processes on macroscopic, mesoscopic and microscopic structural levels and that structure separation

*To whom correspondence should be addressed.

by fracture occurs depending on the starting defect size and the varying crack expansion resistivity.[9] The complexity of fracture-releasing mechanisms in the different structure levels can lead to different trends of strength and fracture toughness as functions of the main microstructural parameters. Therefore, the relation between strength and toughness must be checked for every ceramic separately. In addition, the influence of the sintering parameters, the ceramic composition as well as the crack path and the resulting fracture mode on the Griffith criterion[10–12] must be analysed. A value of 1·26 is used for the geometrical function Y of AlN ceramics.[13–15] The development and the course of the microcracks depend on the intrinsic stresses[10] derived from the different thermal expansion coefficients[16,17] of the AlN matrix ($5{\cdot}5 \times 10^{-6}\,K^{-1}$) and the TiB_2 ($4{\cdot}6 - 6{\cdot}4 \times 10^{-6}\,K^{-1}$) or TiN particles ($9{\cdot}4 \times 10^{-6}\,K^{-1}$).[18] These intrinsic stresses can be calculated by using the relation derived from Wei and Becher,[19] and are constant inside the particles and decrease inside the matrix with increasing distance from the particles. Accordingly, the maximum tangential and radial stresses exist at the boundary between the particles and the matrix, where the radius of the particle is equal to the distance from the particle centre.

In the present paper, the synthesis of particle-reinforced AlN matrix composites and coatings as well as their mechanical and thermal properties are reported. The results are discussed with respect to unreinforced AlN-(4 wt% Y_2O_3) ceramic.

2 Experimental Procedure

2.1 Starting materials

Commercially available AlN powder from Tokuyama Soda Company (Japan) grade F, with mean particle size of approximately 0·6 μm (d_{90} < 2·48 μm), a specific surface area of 3·2 $m^2\,g^{-1}$ and an oxygen content of 0·8 wt%, was used. The employed sintering aid was Y_2O_3 powder from H. C. Starck with a mean particle size of 0·4 μm (d_{90} < 2·5 μm) and a specific surface area of 14 $m^2\,g^{-1}$. As reinforcing particles, TiN and TiB_2 powders from H. C. Starck, grade C and grade F respectively, were used. The particle sizes of TiN and TiB_2 were 1·0 and 0·9 μm and the specific surface areas were 3·7 and 4·1 $m^2\,g^{-1}$, respectively.

2.2 Fabrication and sintering

The composite powders were homogenized by attrition milling of AlN matrix powder, Y_2O_3 sintering aid and TiB_2 or varying contents of TiN reinforcing particles in isopropanol for 1 h at 500 rev min^{-1}. The powder to Al_2O_3 milling ball (diameter < 2 mm) ratio was 1 to 4. The dried composite powders were cold-isostatically pressed (KIP 200, Paul Weber, Germany) into bars (15 mm height, 23 mm width, 60 mm length) and cylinders (23 mm diameter, 22 mm height) with a pressure of 530 MPa for 3 min. Subsequently, the green compacts, placed on sintered AlN ceramic plates, were sintered in a gas pressure furnace (KCE FPW 100/150-2200-50, KCE, Rödental, Germany) with graphite heating elements under a pressure of 0·1 – 0·2 MPa N_2. The heating rate was 10 K min^{-1}, the sintering temperature varied between 1700 and 1900°C, and sintering times at the final temperature were 0, 30 or 60 min. The different powder compositions and their sintering conditions are listed in Table 1.

The reinforced AlN coatings were fabricated by two routes (Table 2). In the first route, a cold-isostatically prepressed AlN-(4 wt% Y_2O_3) green body was coated with the composite powder (25 wt% TiN, 0·5 wt% Y_2O_3) by cold isostatic

Table 1. Composition and sintering temperature and time of the AlN specimens investigated

Sample	*Composition*			*Sintering*		*Density*	
	Y_2O_3 (wt%)	*TiN (wt%)*	*TiB_2 (wt%)*	T *(°C)*	t *(min)*	*Theor ($g\,cm^{-3}$)*	*Rel. (%)*
TB	2·0	0	10	1750	60	3·38	96·5
AN 0·5	0·5	0	0	1700	0	3·27	95·4
AN 2	2·0	0	0	1750	60	3·28	99·4
TN 2-d	2·0	5	0	1750	30	3·35	95·0
TN 2-c	2·0	5	0	1700	30	3·35	95·2
TN 2-b	2·0	5	0	1700	0	3·35	96·2
TN 2-a	2·0	5	0	1650	30	3·35	93·1
TN 0·5-5	0·5	5	0	1700	0	3·33	96·4
TN 0·5-15	0·5	15	0	1700	0	3·46	95·4
TN 0·5-20	0·5	20	0	1700	0	3·53	94·3
TN 0·5-25	0·5	25	0	1700	0	3·61	93·9
TN 0·5-30	0·5	30	0	1700	0	3·68	90·8
TN 0·5-35	0·5	35	0	1700	0	3·76	93·7
TN 4	4·0	25	0	1900	60	3·66	99·9

Table 2. Composition and sintering conditions of layered AlN composites

Sample	*Composition*		*Sintering*	*Hardness*[a]
	Bulk	*Coating*	T/t *(°C)/(min)*	HV 2 *(10^7·Pa)*
A	4 wt% Y_2O_3	25 wt% TiN/ 0·5 wt% Y_2O_3	1700/0	1251
B	4 wt% Y_2O_3	25 wt% TiN/ 0·5 wt% Y_2O_3	1800/0	1260
C[b]	4 wt% Y_2O_3	25 wt% TiN/ 0·5 wt% Y_2O_3	1800/60	1077

[a]Hardness measured at the boundary between the AlN inner body and the composite coating.
[b]In sample C, the bulk was presintered at 1700°C without holding time and 0·1 MPa N_2.

pressing with a pressure of 530 MPa for 3 min. Finally the laminated compact was sintered at a temperature above 1700°C (specimens A and B) in a gas pressure furnace (route 1).[20] In the second route, the cold-isostatically pressed pure AlN body was presintered at 1700°C in 0·1 MPa N_2 and subsequently coated with the composite powder and densified without pressure at 1800°C for 60 min (specimen C, Table 2). In both cases the AlN bodies were placed in the silicone pressing form enveloped with the composite powder.

2.3 Microstructure

The resulting microstructures of the composites were investigated by X-ray diffraction analysis, light-optical microscopy, scanning electron microscopy and energy dispersive X-ray analysis (Zeiss DSM 962 with EDAX, Carl Zeiss, Oberkochen, Germany; Philips SEM 505, Philips, Eindhoven, The Netherlands).

2.4 Mechanical properties

The mechanical properties of the samples were determined as follows. The microhardness *HV* (Leco M-400-G2, Kirchheim, Germany) [21] at 2 kg load (19·61 N) and fracture toughness K_{Ic} were measured by the Vickers indentation method, the latter being calculated according to the method of Anstis *et al.*[22] In addition, K_{Ic} was determined by the single edge notched beam (SENB) method (Instron 1362) according to DIN 51109.[23] Comparison of the fracture toughness values calculated by the indentation method with the corresponding SENB values leads to a value of 0·022 for the so-called material-independent constant for Vickers-released radial cracks[22] for AlN ceramics and composites. The four-point bending strength (Instron 1362) was measured according to DIN 51110 Part 1[24] and the thermal conductivity (WLM 20/105, Dr. Semmler & Reinhart, Meitingen, Germany) by the comparative method according to DIN 51908.[25]

The strength values represent the average of five tested samples.

3 Results

3.1 Densification and sintering

The relative green density of the cold-isostatically pressed samples was about 60%. The densities of the pressureless-sintered bodies reached >95% of the theoretical values for the cylinders and >90% for the bars. The first maximum of the densification rate was observed between 1400 and 1500°C. In this temperature range the secondary yttrium aluminate phases had already been formed. The second maximum of shrinkage was obtained at 1700°C.

The TN 2 specimens containing 2 wt% Y_2O_3 and 5 wt% TiN, sintered under varying temperature–time conditions (1700 ± 50°C; 0 or 30 min) (Table 1), had nearly the same mean fracture strength σ_B of 322–342 MPa (Table 3). In contrast, samples heated to 1700°C without holding time at maximum temperature showed the lowest standard deviation of ± 10 MPa (Fig. 1). The higher standard deviations of ± 50 MPa are mainly caused by the inherent statistical fluctuations, but are also influenced by the low relative density for samples sintered for 30 min at 1650°C or by the larger grain-size distribution for samples sintered at 1700°C/30 min and 1750°C/30 min.

The study of the influence of different amounts of oxide showed that σ_B increases with decreasing Y_2O_3 content down to 0·5 wt%. Based on this result and the fact that the lowest grain-size distribution was obtained at 1700°C/ 0 min (Fig. 1), further investigations were made with samples containing 0·5 wt% Y_2O_3 and varying TiN additions, which were heated to 1700°C without holding time and subsequently cooled down to room temperature (samples TN 0·5). This sintering condition was used to minimize grain growth and to improve bending strength, whereas 1900°C and 60 min (sample TN 4-25) was applied to optimize thermal conductivity.

3.2 Density and Vickers hardness (HV 2)

The density of bar samples of TN 0·5 decreases linearly from about 96% at 0 wt% TiN to 93% at 35 wt% TiN, whereas the *HV 2* increases from 10·5 GPa at 0 wt% TiN to 12·5 GPa at TiN

Table 3. Mechanical and thermal properties of the AlN ceramic composites

Sample	d[a] *(μm)*	HV 2 *(10^7 Pa)*	K_{Ic} *(MPa $m^{1/2}$)*	σ_B[b] *(MPa)*	λ *(W m^{-1} K^{-1})*
TB	5·0	954±34	3·7±0·4	222±13	62·4
AN 0·5	3·5	1067±13	3·4±0·4	262±47	86·2
AN 2	3·8	1070±34	2·6±0·1	267±55	n.d.
AN 4	12·3	870±84	5·0±0·9	n.d.	147·7
TN 2-c	~3·0	1149±18	3·6±0·2	322±40	112·1
TN 2-b	2·0	1206±18	3·4±0·4	342±10	n.d.
TN 0·5-5	1-2	1253±24	3·6±0·3	353±48 390±29[c]	64·9
TN 0·5-15	1-2	1257±19	4·0±0·3	n.d.	62·0
TN 0·5-20	~3	1265[10]±22	4·1±0·3 6·8 SENB	333±41	57·0
TN 0·5-25	1-2	1243±06	4·2±0·5	362±27	56·6
TN 0·5-30	1-2	1251±24	4·6±0·3	323±52	54·9
TN 0·5-35	1-2	1247±31	3·7±0·2 4·0 SENB	232±46	51·6
TN 4-25	7	1074±17	8·3±0·4 8·5 SENB	268±43	106·8

[a]Mean grain size measured by linear cutting method.
[b]Mean four-point bending strength of 5 samples.
[c]353 MPa is the mean strength of 10 samples, whereas 390 MPa is the mean of the 5 best samples.

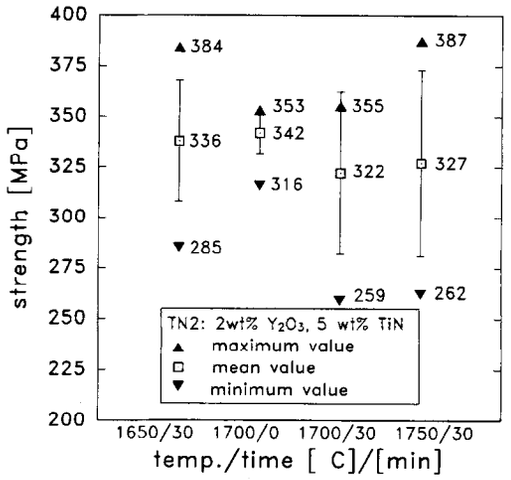

Fig. 1. Four-point bending strength of TN2 composites (see Table 1) as a function of sintering conditions. The error bars show the sample standard deviation.

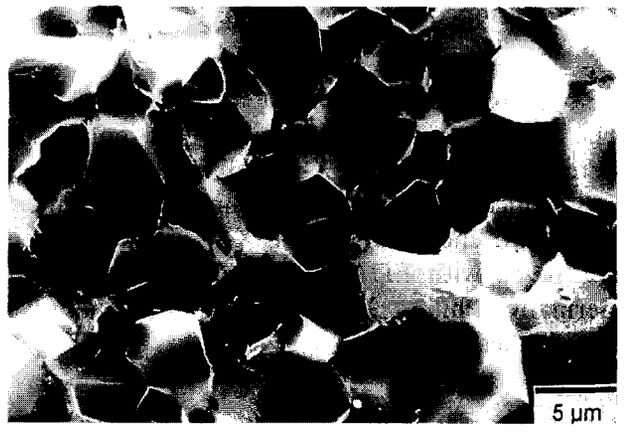

Fig. 2. Scanning electron micrograph of a fracture surface of a pure AlN-(Y_2O_3) ceramic with a large content of intragranular fractured grains.

contents higher than 5 wt%. The relative density and the microhardness *HV 2* of sample TN 4-25 prepared under conditions for high thermal conductivity are 99% and 10·7 GPa, respectively.

The AlN-TiB_2 ceramic composite is characterized by 96·5% of theoretical density and a microhardness of 9·5 GPa.

3.3 Microstructural development

3.3.1 AlN-(Y_2O_3) ceramics

The X-ray diffraction pattern of all sintered specimens without reinforcing particles can be assigned to AlN and $3Y_2O_3{\cdot}Al_2O_3$, $Y_2O_3{\cdot}Al_2O_3$ and/or $2Y_2O_3{\cdot}Al_2O_3$ as the crystalline phases.

The composition AN 0·5 revealed a predominant intragranular fracture path (Fig. 2) whereas sample AN 4 showed an intergranular fracture mode.

3.3.2 AlN-TiB_2 composites

The X-ray diffraction pattern of the AlN–TiB_2 composites can be assigned to AlN, TiB_2 and yttrium aluminate reflections as well as to hexagonal BN reflections. TiN and BN are formed during sintering according to reaction (1):

$$TiB_2 + C + 2\,N_2 \leftrightarrow TiN + 2\,BN + CN\uparrow \quad T_{Tc} \approx 525°C \quad (1)$$

where T_{Tc} means the thermodynamically calculated transformation temperature.[26] Figure 3(a) shows the microstructure of an AlN–TiB_2 composite. The bright TiB_2 grains in the dark AlN matrix have been transformed to TiN and hexagonal BN corresponding to eqn (1). The carbon originates from the furnace atmosphere and the reaction proceeds from the surface to the centre of the grains. The developed BN fibres and plates at the sample surface are shown in Fig. 3(b).

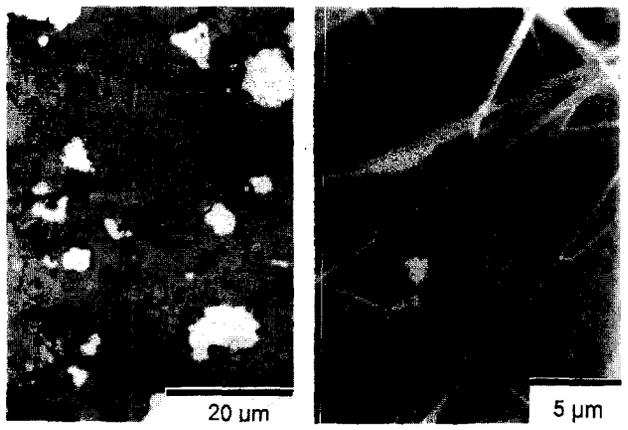

Fig. 3. (a) Light micrograph of a polished microsection (bar = 20 μm) of a TiB_2–AlN composite. The TiB_2 grains (bright) in the AlN matrix (dark) have been transformed to TiN from the edge to the core of the grains. (b) Scanning electron micrograph (bar = 5 μm) of BN fibers and plates as result of the reaction between TiB_2 and N_2.

3.3.3 AlN–TiN composites

The X-ray diffraction pattern of the AlN–TiN composites can be assigned to AlN, yttrium aluminates and TiN. While in the pattern of the samples with low Y_2O_3 contents only the $3Y_2O_3{\cdot}5Al_2O_3$ reflections can be determined, the Y_2O_3-rich sample shows both Y_2O_3 and $2Y_2O_3{\cdot}5Al_2O_3$ reflections.

A comparison of the microstructures of samples TN 0·5-25 and TN 4-25, depicted in Figs 4(a) and 4(b), shows that in both cases the dispersed hard particles (25 wt% TiN) are distributed relatively homogeneously in the matrix. While grain size and morphology in sample TN 0·5-25 [Fig. 4(a)] are similar to those of pure AlN ceramics, the grains of sample TN 4-25 grew to a higher average size and formed globular grains [Fig. 4(b)]. The latter observation suggests that TiN took part in liquid phase sintering.

During sintering at 1900°C for 60 min the TiN particles transformed to TiC from the sample surface to the centre up to a depth of 300 μm. The detail in Fig. 4(c) shows that the reaction from the inner TiN over the intermediate TiCN up to the outer TiC according to reaction (2) is evident:

$$2\,TiN + 2C \leftrightarrow 2\,TiC + N_2 \quad T_{r_c} = 1615°C \quad (2)$$

According to thermodynamic calculations,[26] reaction (2) proceeds at $T \geq 1615°C$ at atmospheric pressure for N_2. Due to the applied N_2 gas pressure (0·1 MPa) in the furnace atmosphere and the fact that the TiN particles are shielded from the atmosphere by the dense sample surface above 1700/1750°C, TiN was stable up to 1800°C.

3.4 Mechanical properties

The mechanical properties of all samples studied are summarized in Table 3.

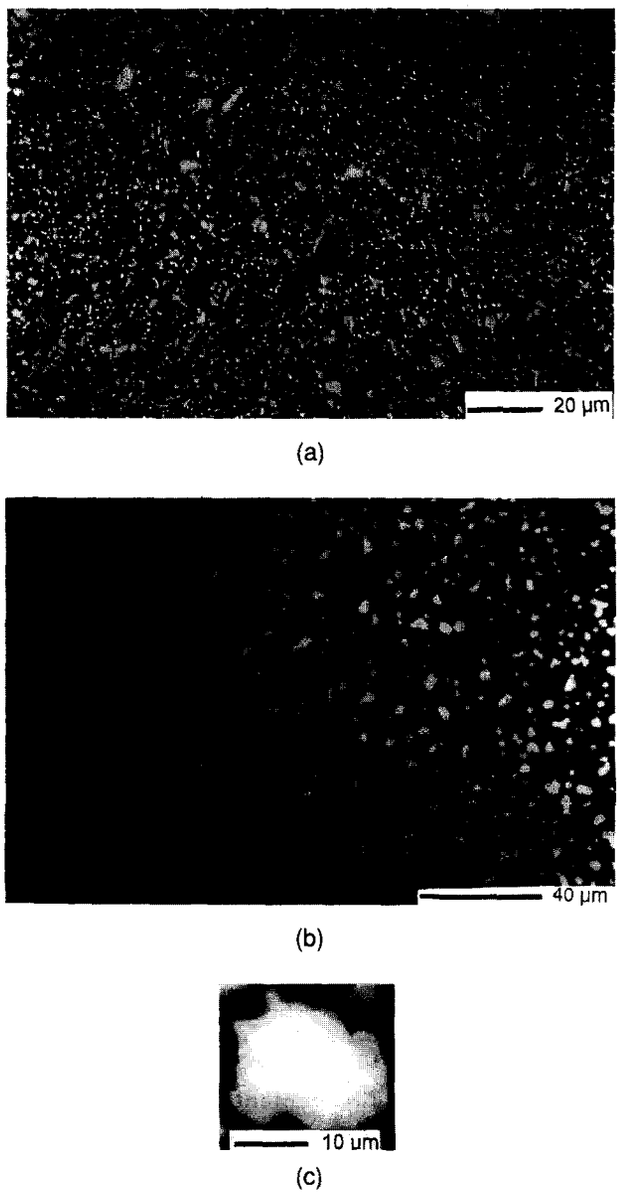

Fig. 4. Light optical micrographs of the polished surface area of (a) TN 0·5-25 (bar = 20 μm) with homogeneously dispersed TiN in the AlN matrix (grey) and (b) TN 4-25 composite (bar = 40 μm), where the TiN grains have reacted to TiCN and to TiC, respectively, from surface to the centre of both the grains (c) and the whole sample (b).

3.4.1 Fracture strength

The mean σ_B values of samples sintered at 1700°C without holding time are presented in Fig. 5 as a function of the TiN content (TN 0·5). The AlN composites containing up to 30 wt% TiN exhibit improved strength values with respect to the unreinforced AlN-(Y_2O_3) ceramic although the relative density of the sintered AlN–TiN material was up to 5% lower. The mean strength increases from 262 MPa to 360 MPa with increasing TiN content. Composites with more than 30 wt% TiN showed a decrease in the mean strength to a value of 232 MPa (Fig. 5). The low σ_B value at 20 wt% TiN is due to the low relative density, which can be related to the low amount of sintering aid (0·5 wt% Y_2O_3).

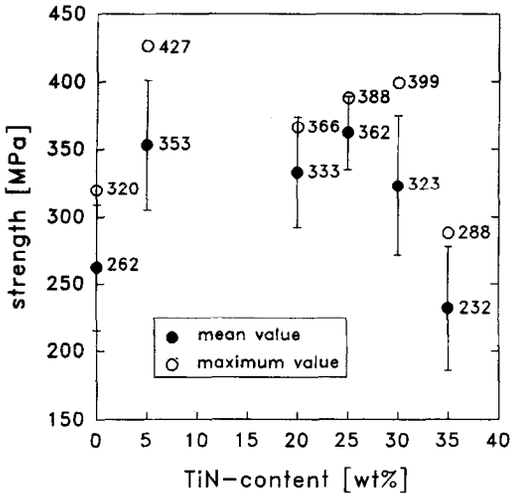

Fig. 5. Mean and maximum four-point bending strengths of the TN 0·5 composites versus TiN content. Error bars show the standard deviation.

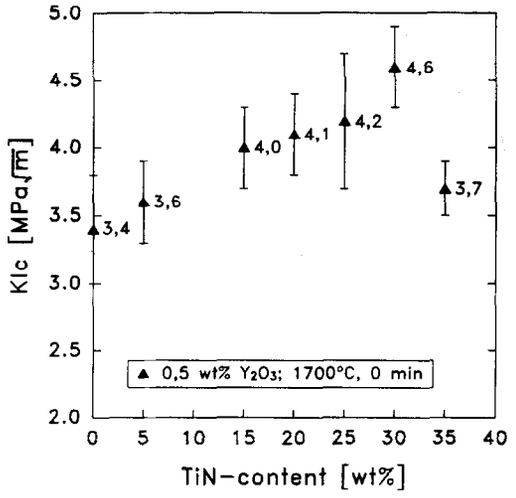

Fig. 6. Fracture toughness of the TN 0·5 composites measured by the Vickers indentation method as a function of TiN content. Error bars show the sample standard deviation.

3.4.2 Fracture toughness

The K_{Ic} value for sample TN 4-25 measured by indentation was 8·3 ± 0·4 MPa $m^{1/2}$, while the TN 0·5 samples have a K_{Ic} of 3·4 to 4·6 ± 0·3 MPa $m^{1/2}$. The fracture toughness measured by the indentation method with a Vickers indenter increases up to 30 wt% TiN approximately linearly from 3·4 to 4·6 MPa $m^{1/2}$ and decreases to 3·7 MPa $m^{1/2}$ at 35 wt% (Fig. 6). The increase can be explained by an enhanced amount of crack deflection with increasing TiN content, while the decrease is due to the low sintering density as a consequence of an insufficient amount of Y_2O_3 compared with the high TiN addition. All composites, TN 0·5 and TN 4, exhibit a higher K_{Ic} than the pure AlN ceramic, AN 2. The K_{Ic} of AN 2 was determined to be 2·6 ± 0·1 MPa $m^{1/2}$ and is in agreement with the values reported in the literature.[1,27]

From Figs 5 and 6 it can be recognized that σ_B and K_{Ic} depend in different ways on the TiN content. The reason for this difference, which has also been reported for other composite systems in the literature,[12] can be explained by the distinct fracture modes of the AlN–TiN composites.

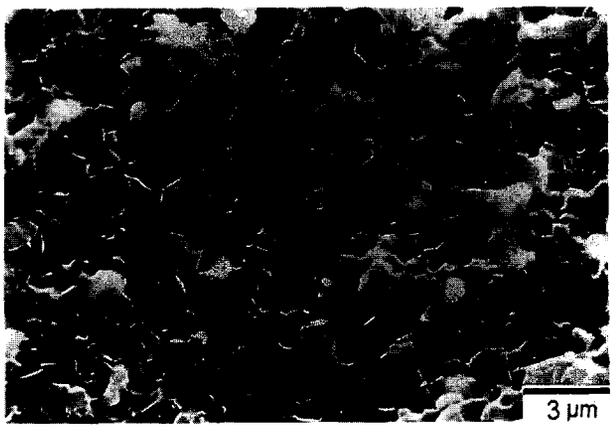

(a)

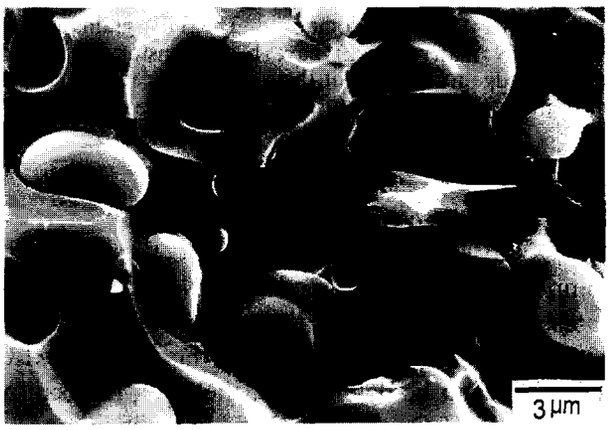

(b)

Fig. 7. Scanning electron micrographs with secondary electron contrast of the fracture surface (bar = 3 µm) of (a) TN 0·5-25 and (b) TN 4.

3.5 Microstructure and mechanical properties of AlN–TiN composites

Figures 7(a) and (b) show the fracture surfaces of two different sintered samples containing 25 wt% TiN. Whereas sample TN 0·5-25 consists of fine-grained AlN and TiN particles with original grain sizes and a transgranular fracture surface of the AlN matrix [Fig. 7(a)], the grains of composite TN 4-25 grew 10 times larger after sintering for 60 min at 1900°C [Fig. 7(b), Table 3]. The difference between these microstructures is related to different Y_2O_3 contents and sintering conditions.

The TiN grains had the globular equilibrium shape and were enveloped with the resulting yttrium aluminate phases. Consequently, the TiN and AlN grains were separated by the yttrium aluminate phases at the grain boundaries, which caused an intergranular fracture mode [Fig. 7(b)].

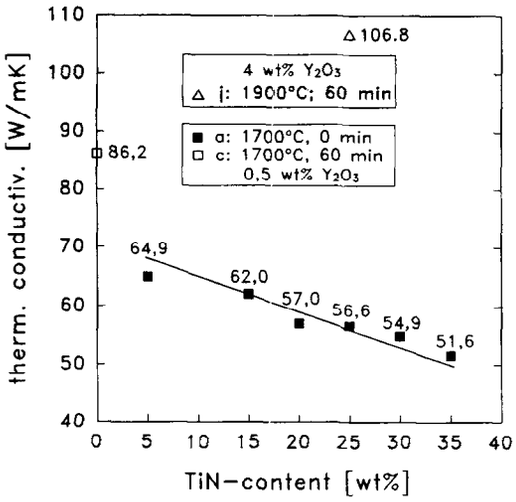

Fig. 8. Thermal conductivity at room temperature of the AlN–TiN composites as a function of TiN content.

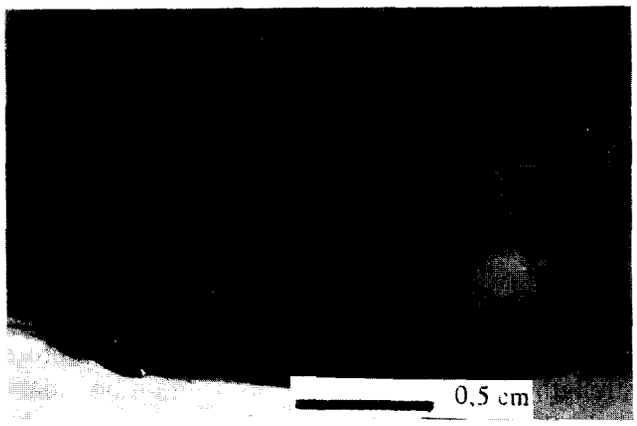

Fig. 9. Light optical micrograph (bar = 0·5 cm) of sample C (Table 2). The AlN-(4 wt% Y_2O_3)/ceramic body was first sintered at 1700°C without holding time and subsequently coated with the AlN-(0·5 wt% Y_2O_3)/25 wt% TiN composite powder.

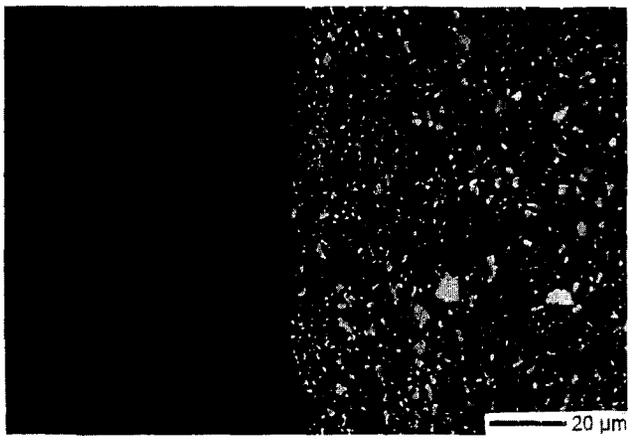

(a)

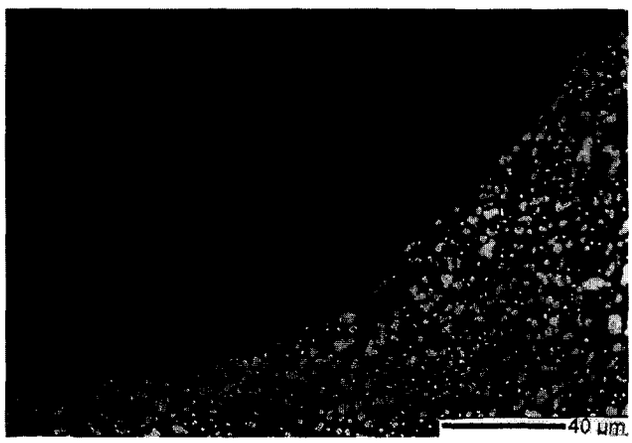

(b)

Fig. 10. Light optical micrographs of the boundary between the AlN bulk material and the TiN reinforced AlN layer of sample B (a) and C (b).

A comparison of the microstructure with the mechanical properties revealed that the fine-grained TN 0·5-25 material with high transgranular fracture path has the higher microhardness and σ_B in spite of the lower density. On the other hand, the coarser microstructure of sample TN 4-25 shows the higher fracture toughness and thermal conductivity (Table 3).

3.6 Thermal conductivity

The thermal conductivities of all samples studied are listed in Table 3.

The thermal conductivity of the fine-grained AlN composites decreased from 86·2 to 51·6 W m^{-1} K^{-1} with increasing TiN content as shown in Fig. 8. This result is due to the low Y_2O_3 content and the low sintering temperature, which is insufficient to purify the AlN grains from oxygen[3] and the whole specimen from the secondary phases at the grain boundaries.

On the other hand, the AlN–TiN composite TN 4-25 had a thermal conductivity of about 107 W m^{-1} K^{-1}. This is 75% of the thermal conductivity of TiN-free AlN ceramics produced by the same sintering conditions (Y_2O_3 content, time, temperature), which was measured to be 150 W m^{-1} K^{-1}.

3.7 Reinforced AlN coatings

Figures 9 and 10 reveal the microstructures of the inner TiN-free AlN ceramic core and the TiN-rich thick coating. Figures 10(a) and (b) show the interface of samples produced according to route 1 (specimens A and B), and route 2 (specimen C) given in Table 2. In the latter case (sample C), the thermal conductivity of the inner pure AlN body is 150 W m^{-1} K^{-1}, whereas the thermal conductivity of the coating is 65 W m^{-1} K^{-1}. Additionally, it can be seen in Fig. 10(a) that a mechanically induced crack crosses the interphase and does not follow the way along the boundary. The Vickers hardness *HV 2* of the laminated AlN bodies was measured to be 1251 and 1260 × 10^7 Pa for samples A and B, and 1077 × 10^7 Pa for sample C at the boundary between the coating and the inner body (Table 2).

4 Discussion

4.1 Fracture mode

According to the theory of linear elastic fracture mechanics,[11,12] the fine-grained microstructure with low amount of oxide additive and intergranular TiN particles (TN 0·5-25) will behave oppositely to the coarse microstructure with high volume of sintering aid and inter- and intragranular TiN particles (sample TN 4-25). With regard to the different fracture mode, the fracture strength and toughness of both the grain boundary and the lattice of the matrix forming the AlN polycrystals have to be considered for an estimation by the linear elastic fracture mechanics (Fig. 11).

Assuming that the strength of the grain boundaries σ_{gb} amounts to 20% of the strength of the pure lattice σ_L,[28] the fracture toughness and strength of an intragranularly broken material with nearly no grain boundary phases are controlled by the lattice. Thus the defect size c of a pore-free microstructure corresponds to the grain size of the material. In the case of an intergranular fracture mode, fracture toughness depends on both the toughness of the grain boundary K_{Ic}^{gb} and of dissipation processes D. The strength of the material is determined by the strength of the grain boundary and the fracture-released defect size corresponds to the size of the grain boundary network. The same rule should be applied to the microhardness.

The conclusion is that composite materials with a fine-grained microstructure and nearly no grain boundary phases lead to high microhardness and high strength, whereas materials with coarse-grained microstructure and a high amount of grain boundary phases lead to high fracture toughness.

4.2 Intrinsic stresses

Crack deflection is one of the dissipation processes that can improve fracture toughness, and can be produced by intrinsic stresses developed by different thermal expansion coefficients of the distinct phases. In the temperature range from 20 to 1000°C TiN has a thermal expansion coefficient of $9{\cdot}4 \times 10^{-6}$ K^{-1}, in contrast to $5{\cdot}5 \times 10^{-6}$ K^{-1} for AlN. Consequently, tensile stresses appear inside the TiN particles and tangential compressive stresses as well as radial tensile stresses in the surrounding AlN matrix. The calculated path of the microcracks is represented in Fig. 12(a).[10,19] The crack deflection caused by the intrinsic thermal misfit stresses can be seen clearly in the microstructure of the composite TN 4-25, which was sintered at 1900°C for 60 min [Fig. 12(b)].[19]

For the case of direct contact between AlN and TiN, these stresses were calculated after Wei and Becher[19] and the results are summarized in Table 4. The estimated radial tensile stresses are of the order of 1000 MPa at the TiN–AlN boundary and 9 MPa at the neighbouring TiN particle for samples with a TiN content of 25 wt%. This explains the low mechanical properties. Moreover, the stresses generated by the superposition of the radial tensile stresses around the TiN particles determine the crack path, because the crack is developed perpendicular to the tensile stresses [Fig. 12(a)].[19]

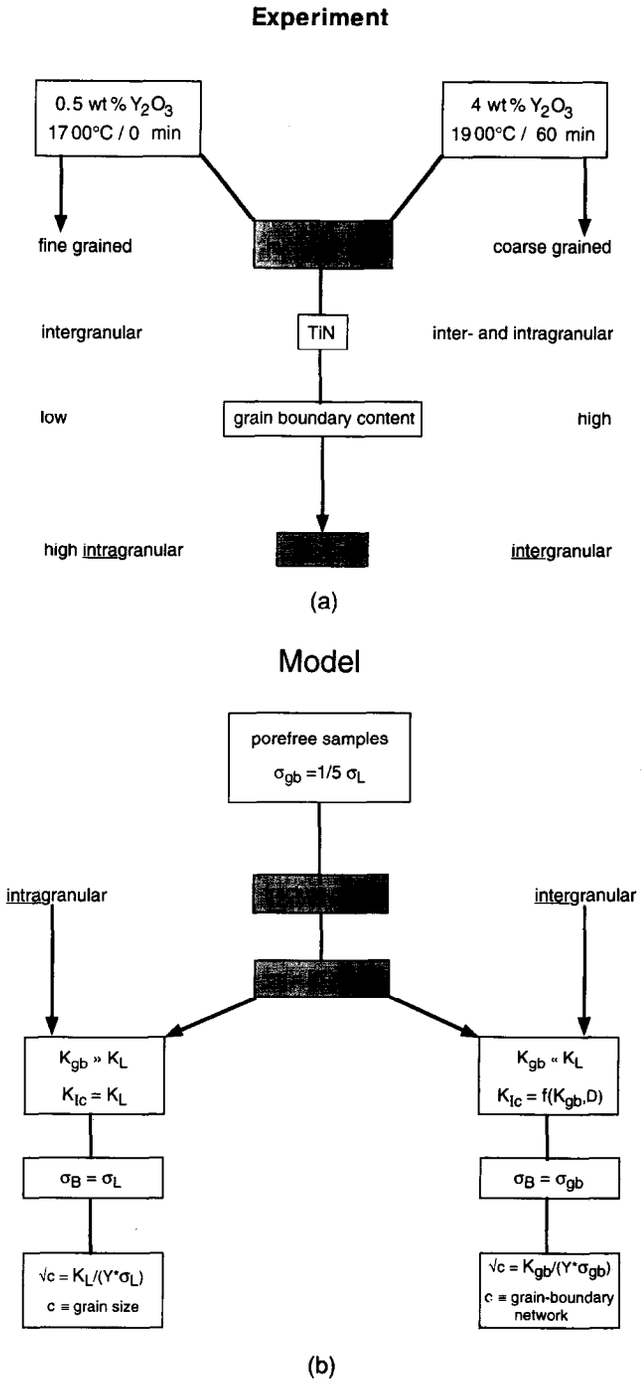

Fig. 11. (a) Flow diagram of the experimental influence of the microstructure of the fracture mode. (b) model for the influence of the fracture mode on the mechanical properties.

4.3 Reinforced AlN coatings

The results of this study revealed that the fracture strength σ_B and fracture toughness K_{Ic} as well as the thermal conductivity λ cannot be optimized simultaneously for the same composition. Therefore, laminated materials with high thermal conductivity inside the sample and high mechanical properties at the surface were developed in the course of this work by the two routes described in Section 2.2 (see Table 2).

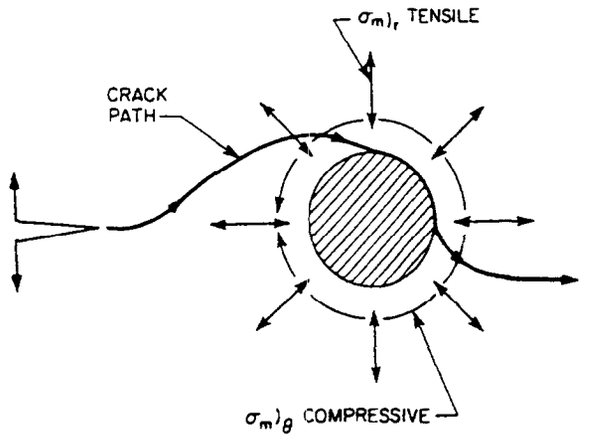

(a)

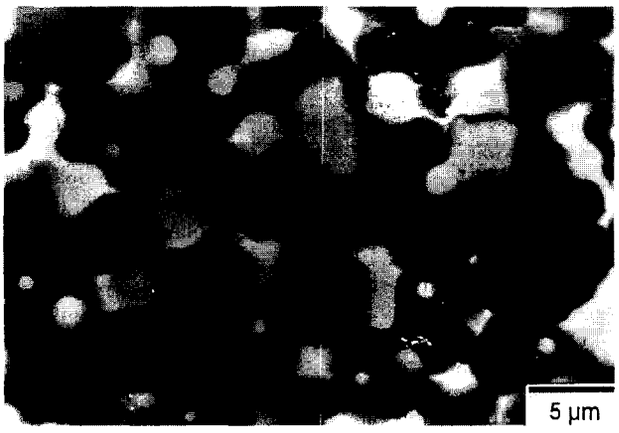

(b)

Fig. 12. (a) Calculated crack path around a globular inclusion as a consequence of a higher thermal expansion coefficient of the particles than the matrix ($\alpha_P > \alpha_M$) after Wei & Becher.[19] (b) SEM micrograph of a crack path of TiN4 induced by a Vickers indentation.

If the sintering temperature of the inner AlN body is higher than that at the surface, especially at route 2, the shrinkage of the coating is higher than that of the inner AlN body. As a consequence cracks can be formed in the coating. Therefore the laminated presintered AlN body was sintered at 1800°C for 60 min, 100°C higher than the sintering temperature of the inner AlN body (sample C). The crack path shown in Fig. 12(b) implies that the adhesion of the composite layer (with a thickness of up to 2 mm) to the inner, pure, AlN core is strong enough to sustain mechanical load.

The higher Vickers hardnesses of samples A and B in contrast to sample C can be attributed to the lower grain size of these samples as a consequence of the lower sintering temperature.

5 Conclusions

The present investigations revealed that TiN is a thermodynamically suitable, stable, hard material to reinforce AlN ceramics. In contrast, TiB_2 reacts with N_2 as the sintering atmosphere to give TiN and hexagonal BN during densification.

The Y_2O_3 and TiN contents as well as the sintering conditions determine the microstructure, the intrinsic stresses, the fracture mode and hence the mechanical properties of the AlN matrix composite.

The four-point bending strength σ_B of the AlN–TiN composites sintered at 1700°C without isothermal hold increases with decreasing Y_2O_3 content as low as 0·5 wt% and increasing TiN

Table 4. Intrinsic stresses developed by thermal mismatch between AlN matrix and dispersed hard material particles, TiB_2 and TiN, calculated according to Wei and Becher[19] (+ tensile stresses, – compressive stresses)

Sample	V_v	r_P/R *(vol%)*	$\sigma_{Mr} = -2\sigma_{Mt}$ *(ΔT = 1000 K) (MPa)*	$\sigma_{dr} = -2\sigma_d$ *(MPa)*
TB	7·63	0·083	–270– +270‡	–0·15– +0·15[a]
TN 2, TN 0·5-5	3·19	3·19	+1008	+0·04
TN 0·5-15	9·90	0·110	+1008	+1·34
TN 0·5-20	13·49	0·156	+1008	+3·83
TN 0·5-25	17·21	0·208	+1008	+9·07
TN 0·5-30	21·09	0·268	+1008	+19·40
TN 0·5-35	25·14	0·336	+1008	+38·24
TN 4-25	17·45	0·211	+1008	+9·47

V_V = volume content of the dispersed hard particles, r_P = radius of the particle, R = distance from the particle centre = mean distance between neighbouring hard material particles at a volume content of V_V, $\sigma_{Mr/t}$ = radial/tangential stresses inside the matrix at the boundary between the particle and the matrix ($r_p = R$), $\sigma_{dr/t}$ = radial (r)/ tangential (t) stresses in the distance corresponding to the next particle centre.

[a]Lowest and highest stresses corresponding to the different thermal expansion coefficients of TiB_2.

additions as high as 25 wt%, whereas the thermal conductivity decreases with increasing TiN content.

The composite containing 4 wt% Y_2O_3 and 25 wt% TiN particles and sintered at 1900°C in 0·1 MPa N_2 exhibits a fracture toughness K_{Ic} of 8 MPa $m^{1/2}$.

Furthermore, AlN/TiN composites with high fracture strength and toughness at the surface and high thermal conductivity (150 W m^{-1} K^{-1}) at the interior were fabricated by coating of an AlN-(4 wt% Y_2O_3) bulk material with a 2 mm thick 25 wt% TiN-particle reinforced AlN layer by pressureless sintering.

Acknowledgement

S.B. gratefully acknowledges the financial support by the grant 'Frauen in den Ingenieurdisziplinen', Ministerium für Wissenschaft und Kunst, Land Hessen and experimental support by Hoechst AG, Frankfurt.

References

1. Kölker, H. & Grellner, W., Aluminiumnitrid — ein neuer Substratwerkstoff. *cfi/Ber. DKG*, **3/4** (1988) 75–79.
2. Komeya, K., Inoue, H. & Tsuge, A., Effects of various additives on sintering of AlN. *Yogyo-Kyokai-Shi*, **89**(6) (1984) 330–336.
3. Buhr, H., Müller, G., Wiggers, H., Aldinger, F., Foley, P. & Roosen, A., Phase composition, oxygen content and thermal conductivity of AlN(Y_2O_3) ceramics. *J. Am. Ceram. Soc.*, **74** (1991) 718–723.
4. Werdecker, W. & Aldinger, F., Aluminum nitride—an alternative ceramic substrate for high power applications in microcircuits. *IEEE Trans. on Components, Hybrids and Manufacturing Technology (CHMT)*, 7(4) (1984).
5. Jiang, D. L., Wang, J. H., Li, Y. L. & Ma, L. T., Studies on the strengthening of silicon carbide-based multiphase ceramics I: the SiC–TiC system. *Mater. Sci. Eng.*, **A109** (1989) 401–406.
6. Hermann, M., Schubert, C., Pabst, J., Richter, H.-J. & Obenaus, P., Gefügeverstärkte Kompositkeramik auf Basis von Si_3N_4. *Verstärkung keramischer Werkstoffe*, DGM Informationsgesellschaft Verlag, 1992.
7. Hong, F., Lumby, R. J. & Lewis, M. H., TiN/sialon composites via in-situ reaction sintering. *J. Eur. Ceram. Soc.*, **11** (1993) 237–239.
8. Martin, C. B., Vivier, P. & Mathieu, P., Electrical discharge machinable ceramic composites. *Mater. Sci. Eng.*, **A109** (1989) 351–356.
9. Woltersdorf, J. & Pippel, E., Grenzflächen- und Mikrostrukturanalyse keramischer Werkstoffe. *Verstärkung keramischer Werkstoffe*, ed. N. Claussen. DGM, 1990.
10. Davidge, R. W. & Green, T. J., The strength of twophase ceramic/glass materials. *J. Mater. Sci.*, **3** (1968) 629–634.
11. Griffith, A. A., The phenomena of rupture and flow in solids. *Phil. Trans. Roy. Soc.*, **221** (1921) 163–198.
12. Wahi, R. P. & Ilschner, B., Fracture behaviour of composites based on Al_2O_3–TiC. *J. Mater. Sci.*, **15** (1980) 875–885.
13. Bansal, G. K., Duckworth, W. & Niez, D. E., Strength–size relations in ceramics materials: investigation of an alumina ceramic. *J. Am. Ceram. Soc.*, **59** (1976) 472–478.
14. de With, G. & Hattu, N., High temperature fracture of hot pressed AlN ceramics. *J. Mater. Sci.*, **18** (1983) 503–507.
15. Zdaniewsky, W. A., Stereoscopic fractography of crack propagation phenomena in a TiB_2–AlN composite. *J. Am. Ceram. Soc.*, **72**(1) (1989) 116–121.
16. Selsing, J., Internal stresses in ceramics. *J. Am. Ceram. Soc.*, **44** (1961) 419.
17. Wiegmann, J., Einfluß des Gefügeaufbaus auf das mechanische Verhalten mehrphasiger Keramikwerkstoffe. *Abh. Akademie der Wissenschaft*, (1978) 288 ff.
18. Munz, D. & Fett, T., Mechanisches Verhalten keramischer Werkstoffe. *WFT Werkstoff-Forschung und-Technik 8*, Springer-Verlag, Berlin–Heidelberg–New York, 1989.
19. Wei, G. C. & Becher, P. F., Improvements in mechanical properties in SiC by the addition of TiC particles. *J. Am. Ceram. Soc.*, **67**(8) (1984) 571–574.
20. Gonia, D. & Schneider, L., Gesinterte Verbundbauteile für Schaltgetriebe. *Beschichten und Verbinden in Pulvermetallurgie und Keramik*, ed H. Kolaska. VDI-Verlag GmbH, Düsseldorf, 1992.
21. DIN 50133, Härteprüfung nach Vickers, 1985.
22. Anstis, G. R., Chantikul, P., Lawn, B. R. & Marshall, D. B., A critical evaluation of indentation techniques for measuring fracture toughness: direct crack measurements. *J. Am. Ceram. Soc.*, **64**(9) (1981) 533–538.
23. DIN 51109, Ermittlung der Rißzähigkeit K_C, 1991.
24. DIN 51110, Teil 1, Prüfung von keramischen Hochleistungswerkstoffen: 4-Punkt-Biegeversuch bei Raumtemperatur, 1990.
25. DIN 51908, Bestimmung der Wärmeleitfähigkeit bei Raumtemperatur nach einem Vergleichsverfahren, 1984.
26. Eriksson, G., Thermodynamic studies of high temperature equilibria. *Chemica Scripta*, **8** (1975) 100–103.
27. Boch, P., Glandus, J. C., Jarrige, J., Lecompte, J. P. & Mexmain, J., Sintering, oxidation, and mechanical properties of hot pressed aluminum nitride. *Ceram. Int.*, **8** (1982) 34–40.
28. Petzold, A., *Anorganisch-nichtmetallische Werkstoffe*. Deutscher Verlag für Grundstoffindustrie, Leipzig–Stuttgart, 1992.